

# Probing the local temperature of a 2DEG microdomain with a quantum dot: measurement of electron-phonon interaction

S. Gasparinetti,<sup>1,\*</sup> F. Deon,<sup>1</sup> G. Biasiol,<sup>2</sup> L. Sorba,<sup>1</sup> F. Beltram,<sup>1</sup> and F. Giazotto<sup>1,†</sup>

<sup>1</sup>*NEST, Istituto Nanoscienza-CNR and Scuola Normale Superiore, Piazza S. Silvestro 12, I-56127 Pisa, Italy*

<sup>2</sup>*CNR-IOM, Laboratorio TASC, Area Science Park, I-34149 Trieste, Italy*

(Dated: June 14, 2022)

We demonstrate that a quantum dot defined in a GaAs/AlGaAs two-dimensional electron gas can be used to probe the local temperature of electrons confined in a microdomain. Our method relies on the observation that a temperature bias across the dot changes the functional form of Coulomb-blockade peaks. In our experimental setup, the dot is tunnel-coupled to a  $16\text{ }\mu\text{m}^2$  electronic domain which is heated by injecting a current through quantum point contacts. Such a device is also a suitable platform for the investigation of electron-energy relaxation at subkelvin temperatures. We find that the energy flux from electrons to phonons is proportional to the fifth power of the temperature, and give a measurement of the electron-phonon coupling constant.

The analysis of the performance and the very understanding of the physical mechanisms governing the behavior of nanostructured devices requires the detailed knowledge of all parameters of electronic systems confined in ever shrinking microdomains. The role of temperature and the investigation of heat transport in solid-state nanoscale systems are currently under the spotlight [1]. Electronic thermometers [2–4], refrigerators [5–8] and heat transistors [9] based on metallic and superconductor nanostructures were already demonstrated. Such devices are typically operated at subkelvin temperatures, where electron-phonon interaction is weak and, as a result, the relevant electronic temperature may significantly differ from that of the lattice (if at all defined). In this context, the ability to perform local measurements of the electronic temperature becomes highly desirable. While in metallic systems superconducting tunnel junctions are routinely employed for this purpose, for the case of two-dimensional electron gases (2DEGs) or semiconductor nanowires at thermal equilibrium, quantum dots (QDs) were shown to be suitable for absolute thermometry [10, 11], due to the fact that in these conditions the linewidth of zero-bias Coulomb blockade (CB) peaks in the weak-coupling regime is directly related to the electronic temperature of the leads.

Here, we propose a method for the detection of the local electronic temperature in a 2DEG, based on the analysis of the CB-peak lineshape. We shall first discuss zero-bias transport through a weakly-coupled QD in the presence of a temperature bias and show that zero-bias conductance measurements can be used to experimentally determine both temperature values. We shall then employ this technique to investigate energy relaxation mechanisms in an electronic microdomain defined electrostatically in a GaAs/AlGaAs heterostructure and heated by an externally-driven current. The domain is connected to the surrounding 2DEG regions through the QD and three quantum point contacts (QPCs). As a known heating power is delivered to the domain, con-

ductance across the QD is probed and the steady-state temperature detected. The dependence of the measured electron temperature on heating power will also be studied for different values of the QPC resistances: as the coupling to the surrounding 2DEG regions is reduced, we observe the crossover from a regime where excess heat is carried away by hot quasiparticles tunneling through the QPCs to one where power exchange with lattice phonons dominates. We shall show that the latter mechanism follows the  $T^5$  power law expected [12] for the screened electron-acoustic phonon piezoelectric interaction, and obtain a measurement of the relative coupling constant consistent with theoretical estimates [1, 13].

Figure 1(a) shows a scanning electron micrograph of the device. Aluminum surface Schottky gates were patterned on the GaAs/AlGaAs heterostructure by electron beam lithography, thermal evaporation and liftoff. The 2DEG is confined 100 nm below the surface and is characterized by a density  $n_s = 2.26 \times 10^{11}\text{ cm}^{-2}$  and a mobility  $\mu = 3.31 \times 10^6\text{ cm}^2/\text{Vs}$ . When a negative voltage is applied to the surface gates, a central domain of area  $A = 16\text{ }\mu\text{m}^2$  is defined by lateral confinement together with a QD and three QPCs. The measurement configuration is schematically shown in the same Fig. 1(a). Experiments were carried out in a  $^3\text{He}$  cryostat down to 250 mK. The domain was heated by driving a dc current  $I_H$  with a floating source through the QPC1-domain-QPC2 circuit while the zero-bias conductance was simultaneously measured across the series QPC3-domain-QD by ac lock-in technique. QPC3 was set to be always much less resistive than the QD so that its voltage drop can be neglected. The single-particle energy-level spacing associated with the lateral dimensions of the domain ( $\pi^2\hbar^2/(2m^*A) \approx 400\text{ neV}$ ) is much smaller than the thermal energy ( $k_B T \approx 21\text{ }\mu\text{eV}$  at 250 mK, where  $k_B$  is the Boltzmann constant and  $m^*$  is the effective mass), so that electrons in the domain can be treated as a Fermi gas. Furthermore, the charging energy of the domain was also found to have negligible impact on the low-bias

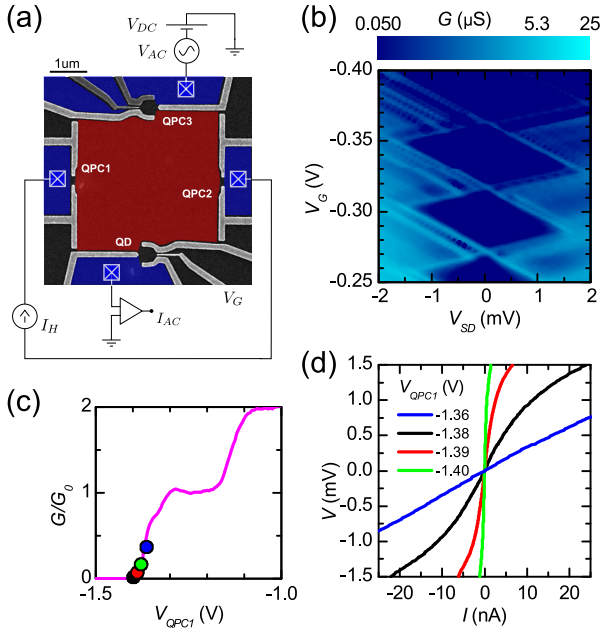


FIG. 1. (a) False-color scanning electron micrograph of the device and scheme of the measurement setup. Aluminum Schottky gates (gray) define a  $16 \mu m^2$  electronic domain (red), which is connected to the outer portions of the 2DEG (blue) through a QD (bottom) and three QPCs (left, right, top). Two additional gates (dark gray) were grounded throughout the measurements. Crossed squares indicate Ohmic contacts to the 2DEG. Two independent circuits are connected to the device: while a floating current source feeds a current  $I_H$  through the series QPC1-domain-QPC2, a differential conductance measurement is performed across the series QPC3-domain-QD. (b-d) Characterization measurements: finite-bias stability plot of the QD (b), zero-bias conductance  $G$  of QPC1 versus gate voltage  $V_{QPC1}$  (c) and current-voltage characteristics of QPC1 for different values of the gate voltage (d); the latter are marked as dots of the same color in panel (c).  $G_0$  is the conductance quantum.

measurements at the temperatures here of interest. Figures 1(b-d) show transport measurements performed on the QD and QPC1 with all other gates set to ground. The QD geometry was chosen in order to maximize its charging energy  $E_C$  and its single-particle energy spacing  $\delta E$ . In the diamonds with lowest occupation number we measured  $E_C = 1.5$  meV and  $\delta E \approx 0.4$  meV [see Fig. 1(b)]. All QPCs show clear zero-bias conductance steps, as shown in Fig. 1(c) for the case of QPC1. Figure 1(d) shows QPC1 current-voltage characteristics at different gate voltages: as the gate voltage approaches pinchoff curves become increasingly non-linear in the given current interval.

Based on the general framework of Ref. [10], we developed a model describing the CB-peak lineshape when a finite temperature bias is applied across the QD. We assumed for the QD a spin-degenerate single-particle energy spectrum and an orbital level spacing exceeding

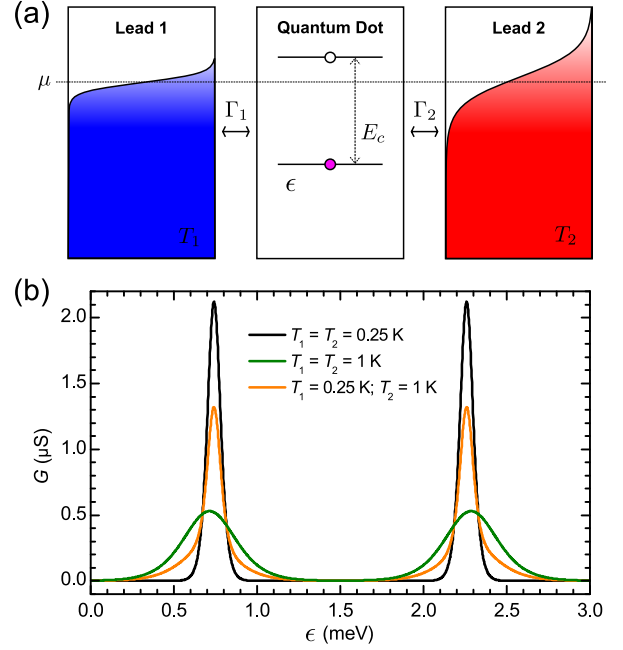


FIG. 2. (a) Energy-level diagram of a temperature-biased QD. The dot is coupled to ideal electron reservoirs at temperatures  $T_1$  and  $T_2$  through tunnel barriers characterized by energy-independent tunneling rates  $\Gamma_{1,2}$ . Transport takes place through a single spin-degenerate level whose energy  $\epsilon$  can be tuned with respect to the chemical potential  $\mu$  by acting on the plunger gate. A finite charging energy  $E_C = 1.5$  meV accounts for on-site electron-electron repulsion. (b) Calculated zero-bias conductance  $G(\epsilon)$  for different temperatures of the leads:  $T_1 = T_2 = 250$  mK (black),  $T_1 = T_2 = 1$  K (green),  $T_1 = 250$  mK and  $T_2 = 1$  K (orange).

thermal energy. As a consequence, only one orbital level contributes to conduction for a given peak and we can model the QD as an Anderson impurity [14, 15] with energy level  $\epsilon$  and on-site interaction  $E_C$ . The dot is tunnel-coupled to ideal leads described by a Fermi-Dirac distribution with chemical potential  $\mu_1$  ( $\mu_2$ ) and temperature  $T_1$  ( $T_2$ ). Coupling is assumed to be weak so that transport is dominated by sequential tunneling and finite-lifetime broadening effects can be neglected. Figure 2(a) provides a sketch of the energy diagram of the dot and the leads in the presence of a temperature bias. Current can be calculated from the master equation for the occupation probability of the QD states. In the limit of large charging energy ( $E_C \gg k_B T_{1,2}$ ) and close to the resonance  $\mu_1 = \mu_2 = \epsilon$  involving occupation numbers  $n = 0, 1$ , we find

$$I(\epsilon) = -2e\Gamma_1\Gamma_2 \frac{f_1(\epsilon) - f_2(\epsilon)}{\Gamma_1 [1 + f_1(\epsilon)] + \Gamma_2 [1 + f_2(\epsilon)]}, \quad (1)$$

where  $f_i(\epsilon) = [1 + e^{(\epsilon - \mu_i)/k_B T_i}]^{-1}$  is the Fermi-Dirac distribution function of the  $i^{\text{th}}$  lead,  $\Gamma_i$  is the tunneling rate between the dot and the  $i^{\text{th}}$  lead and  $e$  is the elec-

tron charge. A similar expression can be found for the peak at  $\mu_1 = \mu_2 = \epsilon + E_C$ , which involves the transition  $n = 1 \leftrightarrow n = 2$ . In the actual device,  $\epsilon$  can be tuned by voltage-biasing the plunger gate ( $V_G$ ). The form of the denominator in Eq. 1 stems from the assumption of spin degeneracy. If a non-degenerate level is considered, then the current reads

$$I(\epsilon) = -2e \frac{\Gamma_1 \Gamma_2}{\Gamma_1 + \Gamma_2} [f_1(\epsilon) - f_2(\epsilon)]. \quad (2)$$

As expected, the well-known result [10] for the zero-bias conductance

$$G(\epsilon) = \frac{e^2}{4k_B T} \frac{\Gamma_1 \Gamma_2}{\Gamma_1 + \Gamma_2} \cosh^{-2} \left( \frac{\epsilon}{2k_B T} \right) \quad (3)$$

is obtained by differentiating Eq. 2 with respect to the source-drain bias in the limit of equal lead temperatures.

Figure 2(b) shows the calculated  $G$  versus  $\epsilon$  in the degenerate case for some representative values of  $T_1$  and  $T_2$ , assuming  $E_C = 1.5$  meV. When  $T_1 = T_2$  temperature variations rescale peaks without affecting their shape (black, green lines). On the contrary in the presence of a temperature bias (i.e.  $T_1 \neq T_2$ ) the line-shape is distorted: peak tails are primarily determined by the higher temperature and the peak body by the lower one (orange line). Notably these qualitative features are common to both Eq. 1 and Eq. 2. This can be understood by noting that Eq. 2 yields a differential conductance proportional to  $-(\partial f_1/\partial \epsilon + \partial f_2/\partial \epsilon)$ . The additional  $\epsilon$ -dependence in the denominator of Eq. 1 introduces an asymmetry in the line-shape and shifts the peak maximum slightly off-resonance.

The presence of this qualitatively different behavior is very useful for a comparison with experimental results. In doing so, we shall assume that the fast electron-electron scattering rate [16] does establish a quasi-equilibrium regime for the confined electron system, so that the microdomain can play the role of the hotter lead. Figure 3(a) shows the measured zero-bias conductance  $G$  versus gate voltage  $V_G$  at  $T_{bath} = 250$  mK. The different curves correspond to increasing heating currents  $I_H$  driven through the QPC1-QPC2 circuit. Here, the device is tuned so that  $R_{QPC1,2,3} \simeq 7.4$  k $\Omega$ , while the conductance of the QD is of the order of a few  $\mu$ S. These experimental characteristics closely resemble the calculated curves of Fig. 2(b). In order to perform a quantitative comparison the derivative of Eq. 1 was fitted to the experimental points [Fig. 3(b)]. The QD barriers were tuned to be symmetric, therefore we put  $\Gamma_1 = \Gamma_2$  in the least-squares fit. Conversion of the gate voltage  $V_G$  into the dot energy  $\epsilon$  was provided by the finite-bias stability plot [11]. Finally after normalizing the curve to the position and value of its maximum, the two lead temperatures are the only free parameters. Following this procedure we can associate two temperatures ( $T_1$  and  $T_2$ , with  $T_2 > T_1$ ) to each measured conductance

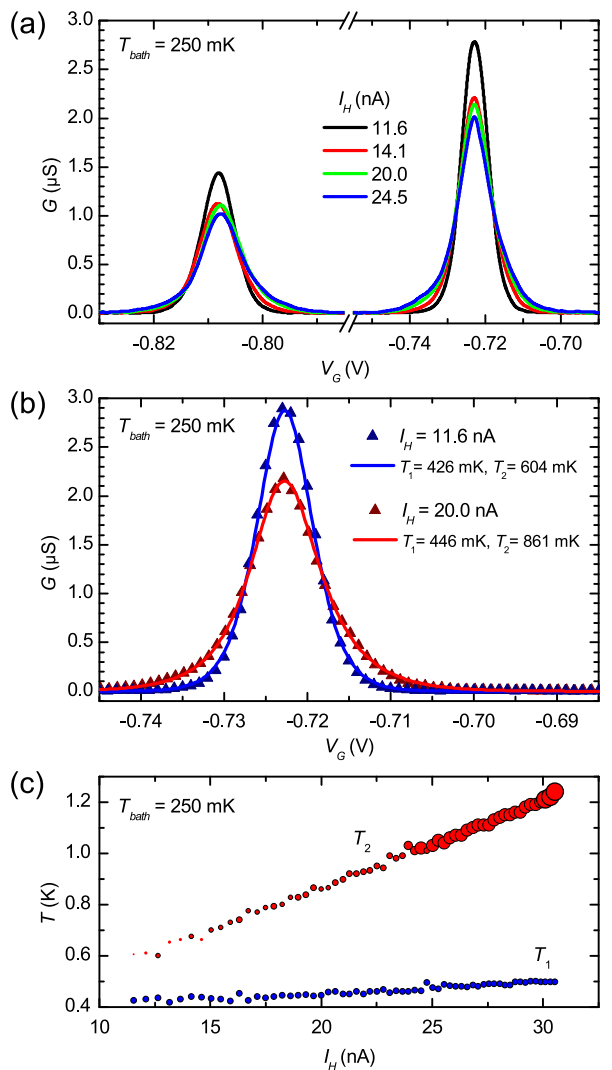


FIG. 3. (a) Experimental traces of the dot conductance  $G$  versus gate voltage  $V_G$  for increasing values of the heating current  $I_H$ , at  $T_{bath} = 250$  mK. (b) Best fit of the derivative of Eq. 1 to the measured CB peak conductance for two values of  $I_H$ . The fits show a good quantitative agreement between theory and experiment, and allow for the extraction of the two temperatures  $T_1$ ,  $T_2$  as the only free parameters. (c) Extracted temperatures  $T_1$  and  $T_2$  as a function of  $I_H$ . The higher temperature ( $T_2$ ) pertains to the heated microdomain, the colder ( $T_1$ ) to the external portion of the 2DEG.

characteristics. Figure 3(c) shows the extracted values of these temperatures as a function of the injection current  $I_H$ .  $T_2$  (in red) steadily increases with  $I_H$ , while  $T_1$  (in blue) exhibits only a small change, its value remaining close to the one measured in an open configuration where only the gates defining the QD are polarized. We assign  $T_2(I_H)$  to the central domain and  $T_1(I_H)$  to the adjacent 2DEG portion. There is a  $\sim 150$  mK difference between the cryostat base temperature and the electronic temperature in the absence of injection that we ascribe to power

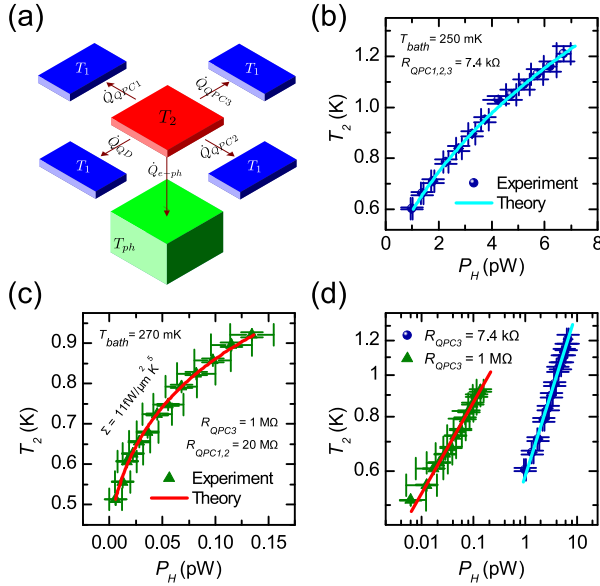


FIG. 4. (a) Scheme of the main contributions to the steady-state power balance. Heat can either flow through the QPCs or be exchanged with the lattice phonons. The QD impedance is set to be so large that its contribution to heat relaxation is negligible. (b-d) Temperature  $T_2$  versus injected power  $P_H$  for different configurations of the device. In (b),  $R_{QPC1,2,3} = 7.4 \text{ k}\Omega$ . The full line is a fit of the power law  $P_H = A + B(T_2^2 - T_1^2)$ . In (c) the zero bias resistances are  $20 \text{ M}\Omega$  for QPC1 and QPC2, and  $1 \text{ M}\Omega$  for QPC3. The continuous line is a fit of the expression  $P_H = C + D(T_2^5 - T_{ph}^5)$ . (d) Joint bi-logarithmic plot of the data in (b) and (c).

leaking through cryostat lines. The additional increase of  $T_1$  with  $I_H$  stems from the global device heating produced by large injection currents. The present procedure allowed us to measure local temperature differences from about 150 mK up to about 1 K. When  $T_1$  and  $T_2$  are too close ( $T_2 - T_1 \lesssim 150 \text{ mK}$ ), the fitting algorithm fails due to the proximity of two symmetrical local minima in the parameter space.

After demonstrating the actual functionality of this thermometry scheme, we can now turn to the investigation of heat relaxation mechanisms in the microdomain. At steady state, electron temperature  $T_2$  is the result of the following thermal-balance equation:

$$\sum_{i=1}^3 \dot{Q}_{QPCi} + \dot{Q}_{QD} + \dot{Q}_{e-ph} = 0, \quad (4)$$

where  $\dot{Q}_{e-ph}$  is the power exchanged between electrons and the phonon bath assumed to be at equilibrium at the cryostat base temperature ( $T_{ph} = T_{bath} = 250 \text{ mK}$ ), while  $\dot{Q}_{QPCi}$  and  $\dot{Q}_{QD}$  are the heat currents flowing through the  $i$ -th QPC and the QD, respectively. Following the notation of Ref. [1], the power flowing out of the domain is given a positive sign. A schematic drawing

of these contributions is shown in Fig. 4(a). We now briefly discuss each term.

The power flow  $\dot{Q}_{QPCi}$  through each QPC can be calculated within the Landauer-Büttiker formalism [17, 18] as an integral over energy involving the total transmission coefficient and the difference between the distribution functions of the two leads. If the transmission coefficient is energy-independent in the relevant range (which also results in a linear current-voltage characteristic), the result can be evaluated analytically. For the biased QPCs it takes the form

$$\dot{Q}_{QPC1} = \dot{Q}_{QPC2} = -\frac{V_H I_H}{4} + \frac{L_0}{2R_{QPC1,2}} [T_2^2 - T_1^2], \quad (5)$$

where  $V_H$  is the total voltage drop developed across the heating circuit,  $L_0 = \pi^2 k_B^2 / 3e^2$  is the Lorenz number and we made use of the fact that  $R_{QPC1} = R_{QPC2}$ . The first term in Eq. 5 is reminiscent of Joule heating. Of the total power  $V_H I_H$  provided by the current source, one half is delivered into the domain,  $P_H = I_H V_H / 2$ . The second term is related to heat leakage from the domain to the (colder) adjacent 2DEG region through quasiparticle tunneling. It is proportional to the difference of the squared temperatures, in agreement with the Wiedemann-Franz law [19]. For the third (unbiased) QPC, only the latter term contributes so that  $\dot{Q}_{QPC3} = (L_0 / 2R_{QPC3}) [T_2^2 - T_1^2]$ .

Let us now turn to  $\dot{Q}_{e-ph}$ , the power transferred through electron-phonon coupling. At low temperatures, heat exchange between the 2DEG and the three-dimensional phonon bath mainly relies on scattering with low-energy acoustic phonons. In particular, for III-V semiconductor alloys, piezoelectric coupling is expected to dominate over deformation-potential interaction [13] at subkelvin temperatures. The energy-loss rate for the screened piezoelectric electron-phonon interaction in the clean limit was calculated [13] and the following dependence on the electron and phonon temperatures was found:

$$\dot{Q}_{e-ph} = \Sigma A (T_2^5 - T_{ph}^5). \quad (6)$$

The coupling constant  $\Sigma$  depends on electron density and on the host-crystal material parameters according to  $\Sigma = n_s [(\zeta(5)(m^* e h_{14})^2) / (64 \pi (2\pi n_s)^{3/2} \hbar^7 \rho q_s^2)] \times ((135/s_l^4) + (177/s_t^4)) k_B^5$ , where  $\rho$  is the mass density,  $h_{14}$  the piezoelectric coupling constant,  $s_l$  ( $s_t$ ) the longitudinal (transverse) sound velocity,  $q_s = m^* e^2 / 2\pi \hbar^2 \epsilon_r \epsilon_0$  is the Thomas-Fermi screening wavevector, and  $\epsilon_r$  and  $\epsilon_0$  are the relative and vacuum permittivity, respectively. By inserting the material parameters of our GaAs/AlGaAs 2DEG [20] we obtain  $\Sigma \approx 35 \text{ fW}\mu\text{m}^{-2}\text{K}^{-5}$ .

In light of the above considerations, the temperature data of Fig. 3(c) are plotted in Fig. 4(b) as a function of the injected power  $P_H$ , evaluated from the measured

$V_H$  and  $I_H$ . The data are well described by the power law  $P_H = A + B(T_2^2 - T_1^2)$ , where  $T_1 = 400$  mK and the constant  $A$  accounts for spurious heating. By fitting this expression to the experimental data we find  $A = (-0.15 \pm 0.02)$  pW, and  $B = (5.0 \pm 0.1)$  pWK $^{-2}$ . This value for  $B$  agrees with the 4.9 pWK $^{-2}$  predicted by Eqs. 4-5 for the heat leakage through three QPCs of equal resistance (7.4 k $\Omega$ ). In this regime, heat flow through the QPCs dominates over electron-phonon heat exchange. As we shall show, increasing the resistance of the QPCs can make their contribution negligible. The data plotted in Fig. 4(c) were taken for a device configuration in which the QPC1 and QPC2 zero-bias resistances were set to 20 M $\Omega$  while that of QPC3 to 1 M $\Omega$ . The continuous line is a fit to the data of the power law  $P_H = C + D(T_2^5 - T_{ph}^5)$ . The good agreement with the experimental data demonstrates the transition to a regime where heat relaxation relies on coupling to the phonon bath. This is manifest in the joint log-log plot of Fig. 4(d), where the two datasets are characterized by different exponents as well as by a different order of magnitude of  $P_H$ . From the least squares fit to the second data series we extract  $C = (-5 \pm 1)$  fW and  $D = (170 \pm 20)$  fWK $^{-5}$ . For our 16  $\mu\text{m}^2$  domain this yields  $\Sigma = (11 \pm 1)$  fW $\mu\text{m}^{-2}$ K $^{-5}$  for the electron-phonon coupling constant, the same order of magnitude of the calculated value.

In conclusion, we have demonstrated that zero-bias conductance measurements on a lateral QD can be used to detect the local electronic temperature of a 2DEG microdomain. Furthermore, we have applied our method to the investigation of heat-relaxation in a GaAs/AlGaAs heterostructure. In particular, our results show that heat exchange between the 2DEG and phonons depends on temperature according to a power law consistent with the screened electron-acoustic phonon piezoelectric interaction, and yielded a measure of the electron-phonon coupling constant. The demonstration of local electronic thermometry as well as the determination of the electron-phonon coupling constant in the subkelvin regime are of crucial importance for the implementation of nanodevices which rely on the manipulation of thermal distributions, e.g. in electronic refrigeration schemes based on QDs [5, 21, 22]. The method here reported can be readily applied to other material systems characterized by different electronic and phononic properties, e.g., InGaAs alloys with high In content [23] or to semiconductor nanowires [24].

We gratefully acknowledge F. Dolcini and S. De Franceschi for fruitful discussions. The work was partially supported by the INFM-CNR Seed project ‘Quantum Dot Refrigeration: Accessing the  $\mu$ K Regime in

Solid-State Nanosystems’, by the NanoSciERA project ‘NanoFridge’, and by the European Community FP7 project No. 228464 ‘Microkelvin’.

\* simone@boojum.hut.fi

† giazotto@sns.it

- [1] F. Giazotto, T. Heikkilä, A. Luukanen, A. Savin, and J. Pekola, *Rev. Mod. Phys.*, **78**, 217 (2006).
- [2] J. Pekola, K. Hirvi, J. Kauppinen, and M. Paalanen, *Phys. Rev. Lett.*, **73**, 2903 (1994).
- [3] N. Appleyard, J. Nicholls, M. Simmons, W. Tribe, and M. Pepper, *Phys. Rev. Lett.*, **81**, 3491 (1998).
- [4] E. Hoffmann, H. Nilsson, J. E. Matthews, N. Nakpathomkun, A. Persson, L. Samuelson, and H. Linke, *Nano Lett.*, **9**, 779 (2009).
- [5] J. Prance, C. Smith, J. Griffiths, S. Chorley, D. Anderson, G. Jones, I. Farrer, and D. Ritchie, *Phys. Rev. Lett.*, **102**, 1 (2009).
- [6] S. Tirelli, A. Savin, C. Garcia, J. Pekola, F. Beltram, and F. Giazotto, *Phys. Rev. Lett.*, **101**, 1 (2008).
- [7] A. Timofeev, M. Helle, M. Meschke, M. Möttönen, and J. Pekola, *Phys. Rev. Lett.*, **102**, 1 (2009).
- [8] S. Kafanov, A. Kemppinen, Y. Pashkin, M. Meschke, J. Tsai, and J. Pekola, *Phys. Rev. Lett.*, **103**, 1 (2009).
- [9] O.-P. Saira, M. Meschke, F. Giazotto, A. Savin, M. Möttönen, and J. Pekola, *Phys. Rev. Lett.*, **99**, 1 (2007).
- [10] C. Beenakker, *Phys. Rev. B*, **44**, 1646 (1991).
- [11] L. P. Kouwenhoven, C. M. Marcus, P. L. McEuen, S. Tarucha, R. M. Westervelt, and N. Wingreen, *Mesoscopic Electron Transport*, edited by L. L. Sohn, L. P. Kouwenhoven, and G. Sch?n (Kluwer, 1997).
- [12] Y. Ma, R. Fletcher, E. Zaremba, M. D’Iorio, C. Foxon, and J. Harris, *Phys. Rev. B*, 9033 (1991).
- [13] P. Price, *J. Appl. Phys.*, **53**, 6863 (1982).
- [14] P. W. Anderson, *Phys. Rev.*, **124**, 41 (1961).
- [15] Y. Meir, N. Wingreen, and P. Lee, *Phys. Rev. Lett.*, **66**, 3048 (1991).
- [16] G. Giuliani and J. Quinn, *Phys. Rev. B*, **26**, 4421 (1982).
- [17] U. Sivan and Y. Imry, *Phys. Rev. B*, **33**, 551 (1986).
- [18] H. Van Houten, L. Molenkamp, C. Beenakker, and C. Foxon, *Semicond. Sci. Tech.*, **7**, B215 (1992).
- [19] M. Switkes, a. G. Huibers, C. M. Marcus, K. Campman, and a. C. Gossard, *Appl. Phys. Lett.*, **72**, 471 (1998).
- [20] M. Brozel and G. Stillman, eds., *Properties of Gallium Arsenide*, Series No. 16, Inspec (Emis Data Reviews, London, 1996).
- [21] H. Edwards, Q. Niu, and A. de Lozanne, *Appl. Phys. Lett.*, **63**, 1815 (1993).
- [22] H. Edwards, Q. Niu, G. Georgakis, and A. de Lozanne, *Phys. Rev. B*, **52**, 5714 (1995).
- [23] F. Deon, V. Pellegrini, F. Carillo, F. Giazotto, G. Biasiol, L. Sorba, and F. Beltram, *Appl. Phys. Lett.*, **96**, 142107 (2010).
- [24] S. De Franceschi, J. a. van Dam, E. P. a. M. Bakkers, L. F. Feiner, L. Gurevich, and L. P. Kouwenhoven, *Appl. Phys. Lett.*, **83**, 344 (2003).